Symmetric and asymmetric membranes based on La0.5Sr0.5Fe0.7Ga0.3O3-δ perovskite with high oxygen semipermeation flux performances and identification of the rate-determining step of oxygen transport

Eva Deronzier, Thierry Chartier, Pierre-Marie Geffroy, P.-M Geffroy

Symmetric and asymmetric membranes based on $La_{0.5}Sr_{0.5}Fe_{0.7}Ga_{0.3}O_{3-\delta}$ perovskite with high oxygen semipermeation flux performances and identification of the rate-determining step of oxygen transport

E. Deronzier[a], T. Chartier [a], P.-M. Geffroy [a]

[a] IRCER, CNRS, Université de Limoges, *CEC, 12 Rue Atlantis, 87068 Limoges, France*

Corresponding author:
Eva Deronzier
Address: IRCER, 12 rue Atlantis, 87068 Limoges
E-mail: eva.deronzier@unilim.fr

Abstract

This work focuses on identifying the rate-determining step of oxygen transport through $La_{0.5}Sr_{0.5}Fe_{0.7}Ga_{0.3}O_{3-\delta}$ membranes with symmetric and asymmetric architectures. The best oxygen semipermeation fluxes are 3.4 10^{-3} $mol.m^{-2}.s^{-1}$ and 6.3 10^{-3} $mol.m^{-2}.s^{-1}$ at 900°C for the symmetric membrane and asymmetric membrane with the modified surface. The asymmetric membrane with a modified surface leads to an increase of approximately 7 times the oxygen flux compared to that obtained with the $La_{0.5}Sr_{0.5}Fe_{0.7}Ga_{0.3}O_{3-\delta}$ dense membrane without surface modification. This work also shows that the oxygen flux is mainly governed by gaseous oxygen diffusion through the porous support of asymmetric $La_{0.5}Sr_{0.5}Fe_{0.7}Ga_{0.3}O_{3-\delta}$ membranes.

Keywords: Oxygen semipermeation, LSFGa5573 perovskite membrane, BSF55 coating, Oxygen diffusion, Porous layer

1 Introduction

Mixed ionic and electronic conductors (MIECs) are used in numerous application areas, such as cathode materials for solid oxide fuel cells (SOFCs) or membrane materials for oxygen gas separation. However, dense ceramic membranes are subjected to critical conditions and have to respond to some criteria. They must present both chemical and dimensional stabilities and suitable mechanical properties at 900°C and under low oxygen partial pressure as well as high oxygen semipermeation fluxes [1]. Currently, no mixed conductors fulfill all these requirements. For instance, strontium-doped lanthanum ferrites present suitable chemical and dimensional stabilities and mechanical resistance at 900°C [1] [2], but oxygen semipermeation fluxes through these materials are too low for potential industrial applications (<1 $ml.cm^{-2}.min^{-1}$ or 7.3 10^{-3} $mol.m^{-2}.s^{-1}$) [1] [3] [4] [5] [6]. By contrast, cobalt and strontium-doped barium ferrites possess low chemical and dimensional stabilities as well as poor mechanical resistance at 900°C [1] [7], but the highest oxygen semipermeation fluxes are obtained for these materials (> 1 $ml.cm^{-2}.min^{-1}$ or 7.3 10^{-3} $mol.m^{-2}.s^{-1}$) [8] [9] [5] [10] [11].

The strategy developed is to associate different materials with satisfying all criteria in specific membrane architectures.
Membranes with surface coatings (or symmetric membranes) consist of a thick dense membrane and thin porous coatings on both membrane surface to improve surface exchanges. Studies [12] [13] reported fluxes obtained on symmetric membranes at 900°C ,2-3 times higher than those obtained on dense membrane without surface modification.
Asymetric membranes consist [14] [15] [16] [17] [18] of a thin dense membrane with a thick porous support . Lee et al. [13] studied a membrane architecture composed of a thick dense membrane and thin porous layers on both membrane sides and achieved an oxygen flux through the symmetric membrane 16 times higher than the dense membrane without porous layers at 900°C under an air/He gradient.

Beside, dual-phase membranes [19] [20] [21] are composed of two materials, an ionic conductor and an electronic or mixed conductor. The ionic conductor used has a fluorine-type structure, very stable material compared to perovskite materials with cobalt. The connected and uniform distribution of these phases is a prerequisite to get a high oxygen semipermeation flux through dual-phase membranes [22]. The microstructure allows two conducting paths for the ions and the electrons. However, dual-phase membranes have been specifically developed to be stable in oxyfuel operating condition where the flux has a lower priority relative to the phase stability [23]. Oxygen semipermeation flux of 1.54 $ml.cm^{-2}.min^{-1}$ ($1.13\ 10^{-2}\ mol.m^{-2}.s^{-1}$) has been obtained through a 60SDC-40SCN (60wt% $Ce_{0.8}Sm_{0.2}O_{2-\delta}$-40wt% $SrCo_{0.9}Nb_{0.1}O_{3-\delta}$) dual-phase membrane at 950°C under an air/He gradient (feed flow rate 120 ml/min, sweep flow rate 60 ml/min) [20].
Some authors [24] [25] [26] [19] combine two types of membrane architectures to get higher oxygen semipermeation fluxes. Zhang et al. [25] investigated a 25µm-thick dense YSZ-LSCrF ($Zr_{0.84}Y_{0.16}O_{1.92}$-$La_{0.8}Sr_{0.2}Cr_{0.5}Fe_{0.5}O_{3-\delta}$) dual-phase membrane supported by a porous support and reported a high flux of 1.58 $ml.cm^{-2}.min^{-1}$ ($1.2\ 10^{-2}\ mol.m^{-2}.s^{-1}$) at 900°C under an air/CO gradient (feed flow rate 100 ml/min, sweep flow rate 35 ml/min). These authors also developed another asymmetric membrane with surface modification and obtained a higher oxygen semipermeation flux of 2.51 $ml.cm^{-2}.min^{-1}$ ($1.8\ 10^{-2}\ mol.m^{-2}.s^{-1}$) in the same operating conditions. Li et al. [26] also reported a high oxygen flux of 1.95 $ml.cm^{-2}.min^{-1}$ ($1.4\ 10^{-2}\ mol.m^{-2}.s^{-1}$) through a sandwich-like symmetric YSZ-LSCrF dual-phase at 900°C under an air/CO gradient (feed flow rate 100 ml/min, sweep flow rate 40 ml/min).

In this work, three membrane designs based on the $La_{0.5}Sr_{0.5}Fe_{0.7}Ga_{0.3}O_{3-\delta}$ (denoted LSFGa5573) material, which corresponds to the best compromise between high oxygen semipermeation fluxes and good chemical stability, were studied. A previous study [12] showed that surface exchange kinetics mainly govern oxygen semipermeation flux through dense LSFGa5573 membranes. Thus, the first configuration consists of a symmetric membrane with coatings added on both membrane surfaces to increase oxygen surface exchange kinetics.
Two other architectures elaborated are asymmetric membranes consisting of a thin membrane layer reinforced by a porous support.
The electrochemical performances of symmetric and asymmetric membranes have been studied thanks to a specific oxygen semipermeation method.

Although asymmetric membranes often show high semipermeation performances [27] [28] [29] [30], the rate-determining step of oxygen transport through the membrane is not clearly identified in the literature.

The novelty of this study is to accurately identify the rate-determining step of oxygen transport in relation with the membrane architecture based on stable cobalt-free materials in operating conditions, such as LSFGa5573 and $Ba_{0.5}Sr_{0.5}FeO_{3-\delta}$ (denoted BSF55) materials. The identification of this rate-determining step allows a better understanding of oxygen transport through the asymmetric membranes in relation with operating conditions and to define specific architectures of membranes to reach improved oxygen fluxes.
This work is also based on the develop of novel asymmetric membranes based on LSFGa5573 material which shows high oxygen semi-permeation performance, good chemical stability and high mechanical properties.

2 Experimental

Figure 1 shows the three membrane architectures studied to improve the oxygen semipermeation fluxes. In addition, this work aims to identify the rate-determining step of oxygen transport concerning these three membrane architectures.

The symmetric membrane consists of a dense $La_{0.5}Sr_{0.5}Fe_{0.7}Ga_{0.3}O_{3-\delta}$ membrane (1 mm thick) coated with $Ba_{0.5}Sr_{0.5}FeO_{3-\delta}$ perovskite on both sides (Figure 1 a).

The asymmetric membranes consist of a dense $La_{0.5}Sr_{0.5}Fe_{0.7}Ga_{0.3}O_{3-\delta}$ membrane (approximately 0.15 mm thick) supported by a thick porous $La_{0.5}Sr_{0.5}Fe_{0.7}Ga_{0.3}O_{3-\delta}$ layer (approximately 0.85 mm thick), without (Figure 1 b) or with a thin porous $La_{0.5}Sr_{0.5}Fe_{0.7}Ga_{0.3}O_{3-\delta}$ layer on the opposite membrane surface (Figure 1 c).

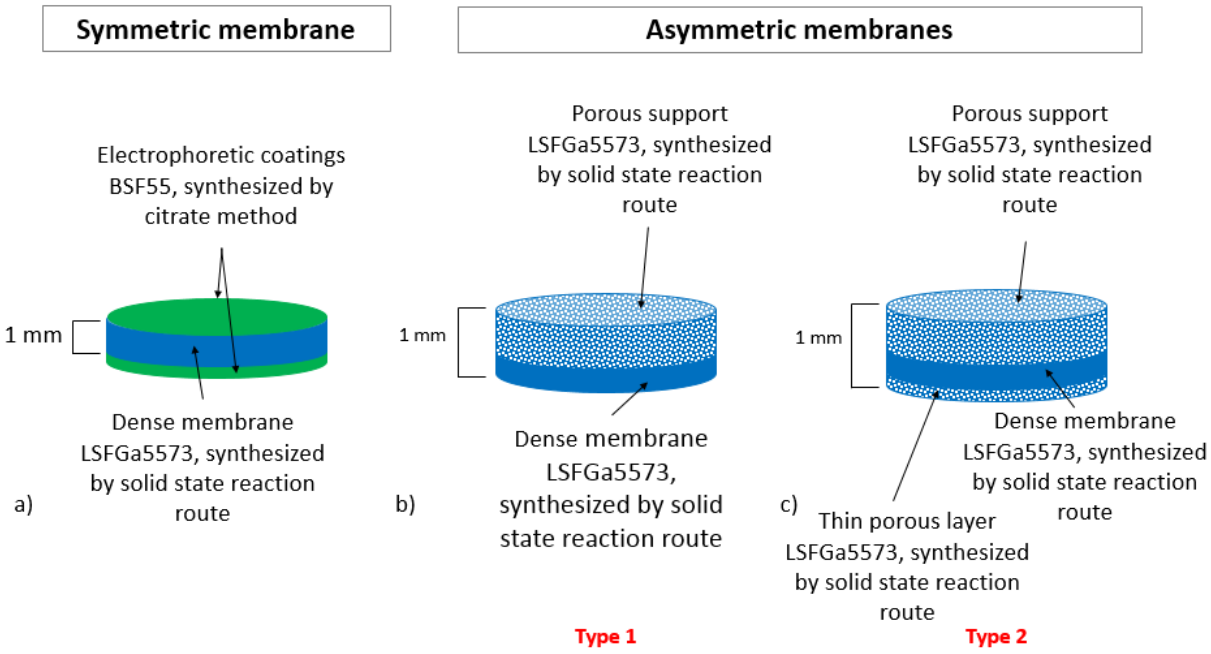

Figure 1: The three studied membrane architectures: symmetric membrane (a), asymmetric membranes without (b), and with thin porous layer (c)

2.1 Elaboration of symmetric membranes

The elaboration of symmetric membranes (Figure 1 a) consists of elaborating dense La0.5Sr0.5Fe0.7Ga0.3O3-δ membranes $Ba_{0.5}Sr_{0.5}FeO_{3-\delta}$ coatings on both membrane surfaces.

2.1.1 Dense LSFGa5573 membrane

LSFGa5573 perovskite powder was synthesized by the solid-state reaction route from pure oxide or carbonate precursors, i.e., La_2O_3 (99.99%, Alfa Aesar), Fe_2O_3 (98%, Alfa Aesar), Ga_2O_3 (99.999%, Alfa Aesar), and $SrCO_3$ (99.9%, Sigma-Aldrich). The synthesis was described in a previous study [31].

The LSFGa5573 membranes were manufactured by the tape-casting process, published earlier [31] [32]. The green membranes were debinded and sintered at 1380°C for 4 h to obtain a relative density higher than 95% (Archimedes' method).

2.1.2 Electrophoretic coatings on LSFGa5573 dense membranes

The $Ba_{0.5}Sr_{0.5}FeO_{3-\delta}$ (BSF55) perovskite powder was synthesized by the citrate method from pure nitrate precursors, i.e., $Ba(NO_3)_2$ (99+%, Alfa Aesar), $Sr(NO_3)_2$ (99.0% min, Alfa Aesar) and $Fe(NO_3)_3.9H_2O$ (98+%, Alfa Aesar). The synthesis was described in a previous study [12].

The preparation of the BSF55 suspension for electrophoretic coatings was detailed earlier [12]. The setup of electrophoretic deposition is shown in Figure SI in Supplementary information section. This setup is composed of a generator (Keithley 2400) and a beaker of 150 ml, which contains the suspension. Two electrodes were dropped in the suspension: a copper electrode and crocodile plier cathodic membrane. The distance between these two electrodes was fixed to 2 cm. A voltage of 20 V was applied, and the deposition time was 1 min. The coatings were carried out under magnetic stirring to prevent the eventual sedimentation of the suspension. After deposition, coatings were dried at room temperature for 48 h. Then, coated membranes were calcined at 1000°C for 1 h at a rate of 1°C/min to remove organic additives and consolidate the coating. Coated membranes were observed using scanning electron microscopy (JEOL IT 300 LV).

2.2 Elaboration of asymmetric membranes

Two architectures of asymmetric membranes were produced in this work, as reported in Figure 1 b) and c). The first type of asymmetric membrane architecture comprises thick porous support and a thin dense membrane (asymmetric membrane without thin porous layer: type 1). The second type of asymmetric membrane architecture comprises thick porous support in contact with the oxygen-rich side, a thin dense membrane, and a thin porous layer in contact with the oxygen lean side (asymmetric membrane with thin porous layer: type 2).

Asymmetric membranes were obtained by a tape-casting process. Two suspensions (including/excluding wood flour) used as pore-forming agents were prepared from LSFGa5573 powder synthesized by a solid-state reaction route. The procedure to obtain suspension and green tapes was published earlier [31] [33]. Porous and dense discs are stacked and laminated under a pressure of 50 MPa at 70°C. The green membranes were

debinded and sintered at 1380°C for 4 h. Asymmetric membranes were observed using scanning electron microscopy (JEOL IT 300 LV).

2.3 Characterizations of powders and membranes

X-ray diffraction patterns, were carried out at room temperature under air on calcined powders with a D8 advance diffractometer with CuKα1. The patterns were recorded in the 10-70° 2θ range with a step of 0.02° and exposure time of 1.1 s per step.
After debinding and sintering, the membrane microstructures were observed using scanning electron microscopy (JEOL IT 300 LV). The tape-casting process allows to obtain a good surface finish, so the membranes surface has not been polished. The grain and pore size and the porosity of sintered membranes were evaluated from observations of membranes surface and cross-section by scanning electron microscopy (SEM).

The oxygen semipermeation flux was measured using a homemade setup described in previous studies [34] [1]. A membrane architecture (1 mm thick and 24 mm diameter after sintering) was sealed between two alumina tubes with gold O-rings to obtain an airtight system. The membrane architecture was submitted to an oxygen partial pressure gradient. The membrane architecture's feed side was flushed with an air (pO_2=0,21 atm) flow of 100 ml/min, and the permeate side was flushed with an argon (pO_2=10^{-4}-10^{-5} atm) flow of 200 ml/min. Measurements were performed between 400°C and 950°C.

3 Results and discussion

3.1 Symmetric membrane samples

3.1.1 DRX and SEM characterizations

The LSFGa5573 powder has a main perovskite phase and two secondary phases, La_2O_3 and $SrLaGa_3O_7$. The BSF55 powder shows a pure perovskite phase. Diffraction patterns are presented in figure SII in Supplementary information.

The architecture obtained by tape casting and electrophoretic deposition given in Figure 2 shows, on a dense LSGa5573 membrane, a homogeneous BSF55 coating with a thickness of approximately 15 µm (Figure 2 c)) and composed of grains smaller than 2 µm (Figure 2 a) and b)).

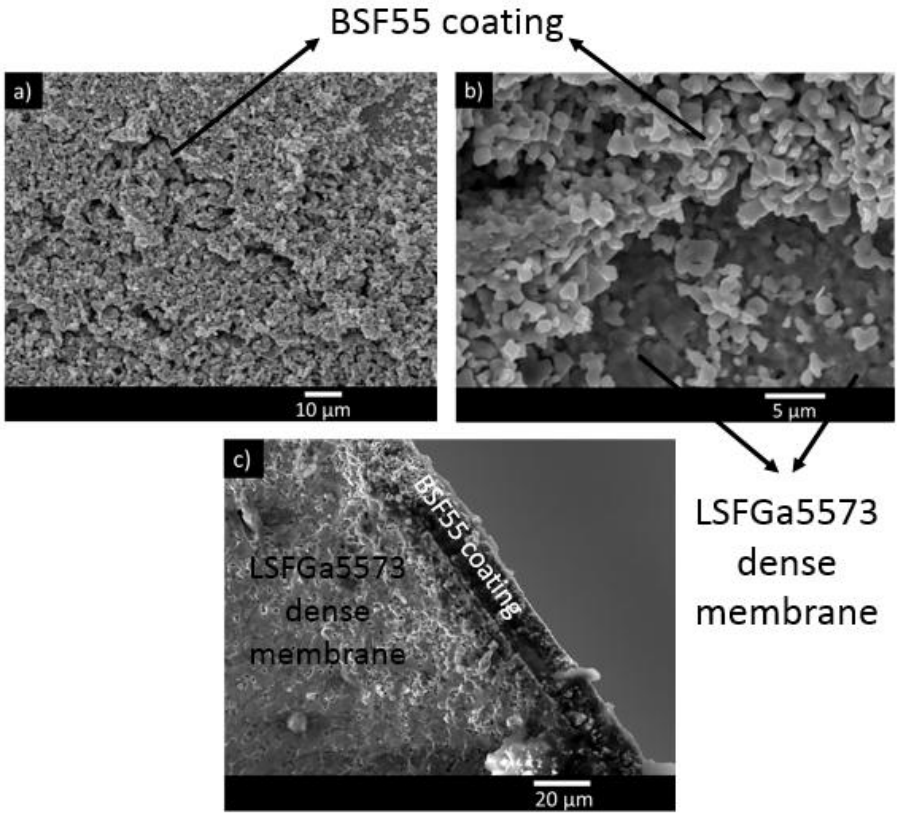

Figure 2: Microstructure of the symmetric membrane with porous layer a), b) on the surface top and the cross-section c)

3.1.2 Electrochemical performances through symmetric membranes

Figure 3 a) shows the evolution of oxygen semipermeation flux versus the symmetric membrane's temperature based on LSGa5573 and BSF55 materials. The flux of 3.4 10^{-3} mol.m^{-2}.s^{-1} at 900°C, is four times higher than that obtained from the dense LSFGa5573 membrane (Table 1).

Furthermore, the oxygen flux obtained from the symmetric membrane in this work is only 1.3 times higher than that obtained by Guironnet et al. [12] for a symmetric LSFGa5573 membrane with a $La_{0.6}Sr_{0.4}Fe_{0.8}Co_{0.2}O_{3-\delta}$ coating and almost 3 times higher than that obtained by Reichmann et al. [34] for a symmetric membrane with a $La_{0.5}Sr_{0.5}Fe_{0.7}Ga_{0.3}O_{3-\delta}$ coating (Table 1). Indeed, the coefficient of surface exchange of coating materials for symmetric membranes has a low influence on the oxygen flux because the oxygen flux is primarily governed by oxygen diffusion through the dense layer in symmetric membranes.
Lee et al. [13] also reported that the flux through a symmetric $La_{0.7}Sr_{0.3}Fe_{0.6}Ga_{0.4}O_{3-\delta}$ membrane with a $La_{0.6}Sr_{0.4}CoO_{3-\delta}$ coating is three time higher than for the dense $La_{0.7}Sr_{0.3}Fe_{0.6}Ga_{0.4}O_{3-\delta}$ membrane.

In addition, Pan et al. [35] reported that the oxygen flux obtained through the membrane architecture with a 10 µm-thick LSFCo6482 coating is 2 times higher than that obtained from dense hollow fibre without coating and 3 times higher for a $Ba_{0.5}Sr_{0.5}Fe_{0.2}Co_{0.8}O_{3-\delta}$ (BSFCo5528) coating. Thus, barium-based materials allow the enhancement of even more kinetics of surface exchange than lanthanum-based materials.

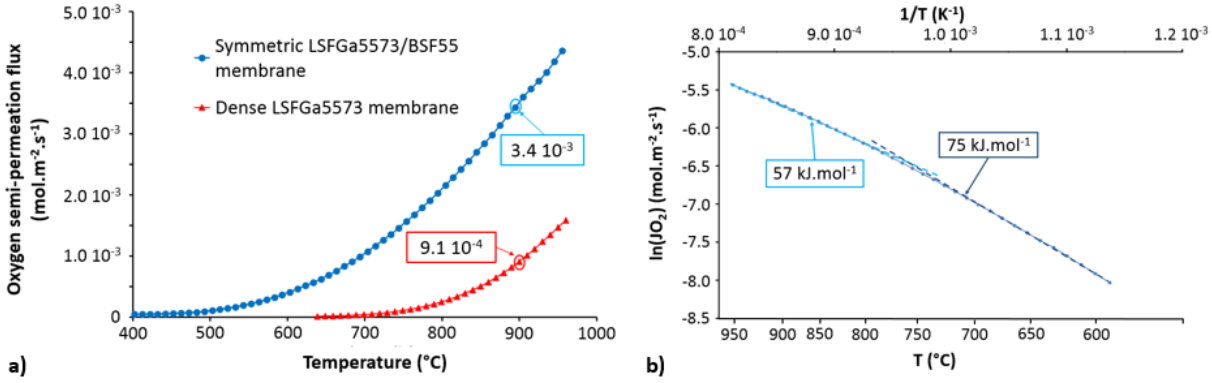

Figure 3: a) Temperature dependence of the oxygen semipermeation fluxes (JO_2) through the symmetric LSFGa5573/BSF55 membrane and the dense LSFGa5573 membrane under an air (100 ml.min^{-1})/argon (200 ml.min^{-1}) gradient, b) Arrhenius plot of oxygen flux versus *1/T of the symmetric LSFGa5573/BSF55 membrane*

Table 1: Activation energies and oxygen semipermeation fluxes through symmetric membranes and dense membranes without coatings at 900°C

Dense membrane material/ Thickness	**Coating material/ Process/ Thickness**	**Reference**	**pO_2 in oxygen rich/lean chamber (atm.)**	**Oxygen semi-permeation flux (mol.m^{-2}.s^{-1})**	**Activation energy at high and low temperatures (kJ.mol^{-1})**
$La_{0.5}Sr_{0.5}Fe_{0.7}Ga_{0.3}O_{3-\delta}$/ 1 mm	$Ba_{0.5}Sr_{0.5}FeO_{3-\delta}$/ Electrophoretic method/ 15 µm	This work	0.21/6.9 10^{-3}	3.4 10^{-3}	57 (760-960°C) 75 (600-760°C)
$La_{0.5}Sr_{0.5}Fe_{0.7}Ga_{0.3}O_{3-\delta}$/ 1 mm	$La_{0.6}Sr_{0.4}Fe_{0.8}Co_{0.2}O_{3-\delta}$/ Electrophoretic method/ 115 µm	Guironnet et al. [12]	Air/Argon	2.6 10^{-3}	51 (800-960°C) 60 (620-800°C)
$La_{0.5}Sr_{0.5}Fe_{0.7}Ga_{0.3}O_{3-\delta}$/ 1 mm	-		Air/Argon	8.5-9.5 10^{-4}	120 (820-970°C) 155 (640-820°C)
$La_{0.5}Sr_{0.5}Fe_{0.7}Ga_{0.3}O_{3-\delta}$/ 1 mm	$La_{0.5}Sr_{0.5}Fe_{0.7}Ga_{0.3}O_{3-\delta}$/ Dip-coating method/ -	Reichmann et al. [34]	Air/Argon	1.2 10^{-3}	-
$La_{0.7}Sr_{0.3}Fe_{0.6}Ga_{0.4}O_{3-\delta}$/ 1.7 mm	$La_{0.6}Sr_{0.4}CoO_{3-\delta}$/ Screen-printing method/ 2-3 µm	Lee et al. [13]	Air/He	5.5 10^{-4}	-
$La_{0.7}Sr_{0.3}Fe_{0.6}Ga_{0.4}O_{3-\delta}$/ 1.7 mm	-		Air/He	1.83 10^{-4}	-

Figure 3 b) shows the Arrhenius plot of oxygen semipermeation flux versus 1/T (T: absolute temperature in K) for the symmetric membrane. The Arrhenius plot's slope gives the activation energy (Ea) corresponding to the rate-determining step (rds) of oxygen transport through the membrane. A variation in the slope of the Arrhenius plot is observed between 750°C and 800°C. Two activation energies of rds can be determined: one at high temperature (>800°C) and one at low temperature (<750°C). The lower activation energy at high temperature (>800°C) for the symmetric membrane in this work is close to that obtained from the membrane architecture reported by Guironnet et al. [12] (Table 1). At 900°C, the oxygen chemical potential profile through the LSFGa5573/BSF55 symmetric membrane (Figure 4) presents a large gradient of oxygen chemical potential in the membrane bulk, suggesting that the oxygen semipermeation flux is mainly governed by mechanisms of oxygen bulk diffusion, as expected.

At low temperatures (<750°C), the activation energy is slightly higher, corresponding to a slight evolution towards a mixed regimen when the temperature decreases. However, this value of activation energy at low temperatures is still close to that obtained at high temperatures, suggesting no significant evolution of the rate-determining step over the full temperature range studied in this work (550-950°C).

In conclusion, the oxygen flux through the dense LSFGa5573 membrane without coating is mainly governed by surface exchange mechanisms. The BSF coatings on the dense LSFGa5573 membrane led to a significant increase in oxygen surface exchange kinetics. Thus, the oxygen flux through the symmetric membrane becomes mainly governed by bulk oxygen diffusion through the membrane (Figure 4).

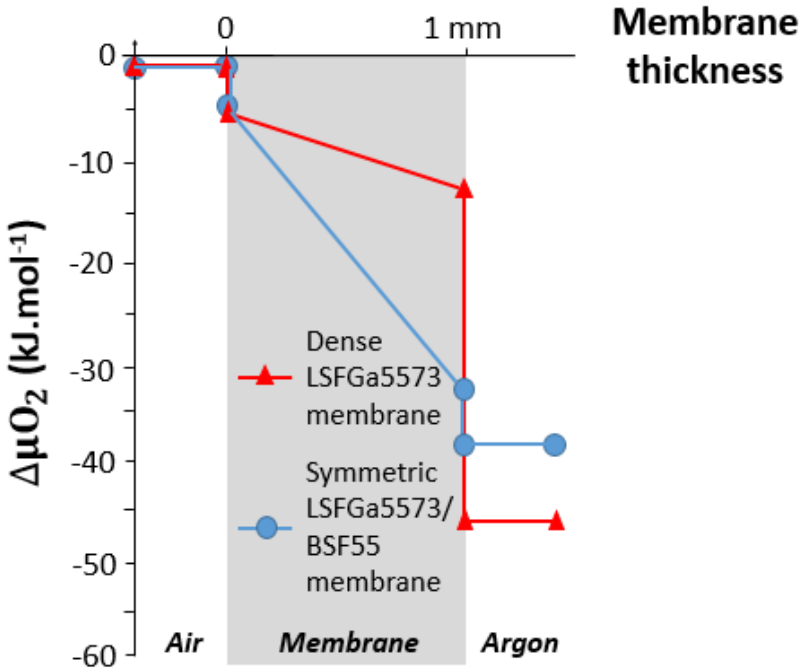

Figure 4: Profiles of the oxygen chemical potential (μO_2) through dense LSFGa5573 membrane and symmetric LSFGa5573/BSF55 membrane at 900°C

3.2 Asymmetric membrane samples

Oxygen semipermeation fluxes through the symmetric membrane architecture are mainly governed by oxygen bulk diffusion through the membrane, assuming the decrease in the dense membrane thickness leads to an increase in the oxygen fluxes. Thus, asymmetric membrane architectures have been produced from a thin dense layer and thick porous support (Figure 1 b) and c)) to ensure the membrane's mechanical resistance.

3.2.1 SEM characterizations

The porous layers of the two asymmetric membrane architectures were obtained using wood flour as a pore-forming agent, presenting acicular grains. The grain length varies between 10 and 300 µm (figure SIII in Supplementary information section). After debinding and sintering of the membranes, the thick porous support and the thin porous layer show pores of a few micrometers with an acicular shape and a porosity of approximately 25-30%, which is interconnected and homogeneous in the whole bulk of the thick support or the thin layer (Figure 5). Table 2 shows membrane characteristics: the thickness of porous and dense layers and the acronyms used in this work.

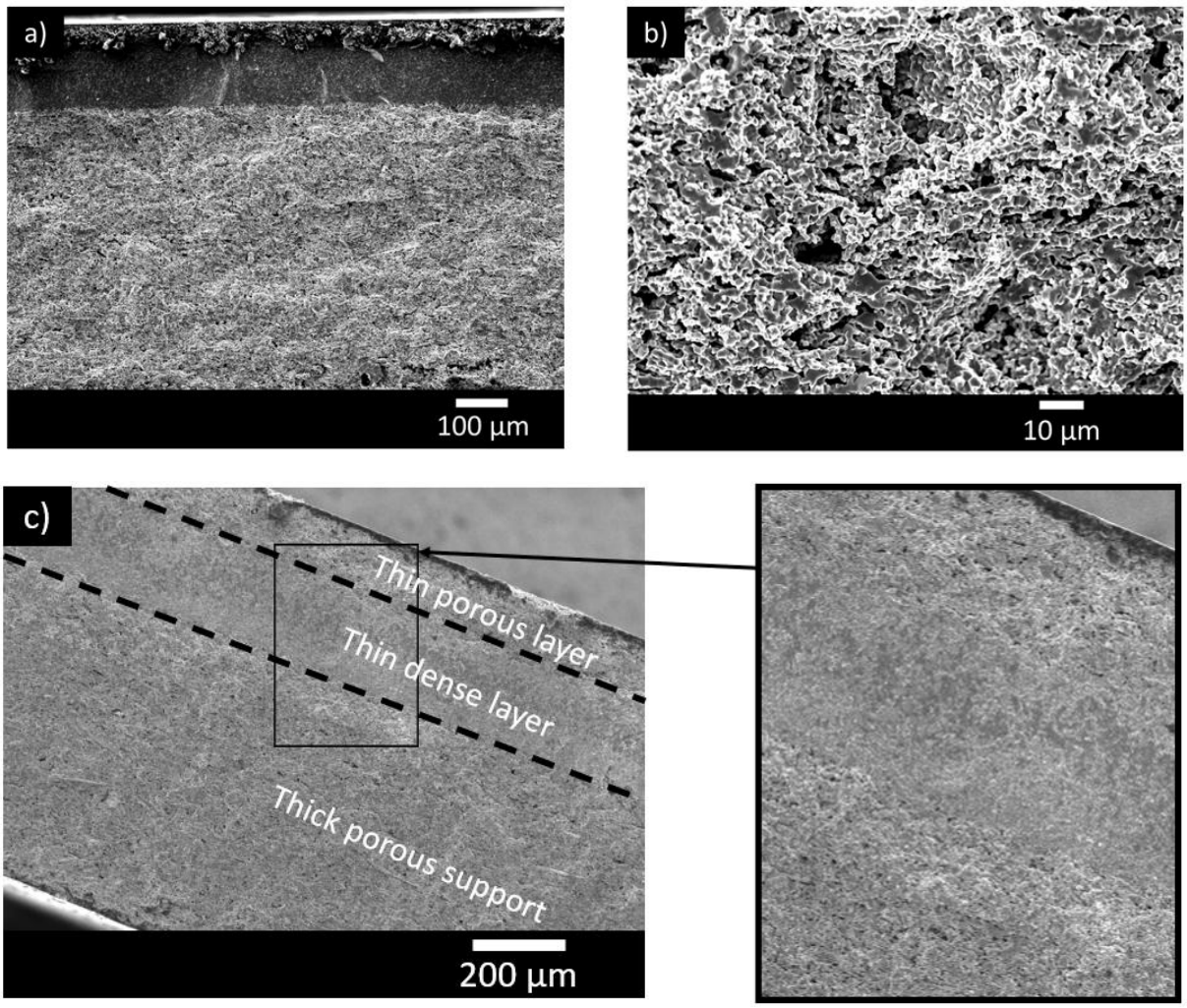

Figure 5: Cross-section of asymmetric membrane a) and thick porous layer b) and asymmetric membrane with modified surface c)

Table 2: Characteristics of asymmetric membranes developed in this work

Thickness of the dense membrane	Thickness of support/thin layer	Atmosphere in contact with the thick porous support	Type of architecture	Notation
170-230 µm	750-800 µm/0 µm	Air	Asymmetric membrane of type 1 (without thin porous layer)	PS-air*
170-230 µm	750-800 µm/0 µm	Argon	Asymmetric membrane of type 1 (without thin porous layer)	PS-Ar**
170-230 µm	500-550 µm/ 150-200 µm	Air (configuration A)	Asymmetric membrane of type 2 (with thin porous layer)	PS-PL***

*PS-air: Porous support (PS) in contact with air side

**PS-Ar: Porous support (PS) in contact with Argon side

***PS-PL: Porous support (PS) in contact with the air side and porous layer (PL) in contact with the argon side

3.2.2 Electrochemical performances through asymmetric membranes

The porous support of asymmetric membranes of flux type 1 (without a thin porous layer) can contact the oxygen-rich or lean sides following the configuration of gas circulation in the setup. Figure 6 a shows the oxygen semipermeation fluxes through asymmetric membranes of type 1 as a function of the temperature and for both configurations (the porous support in contact with oxygen-rich or lean sides). In both cases, oxygen fluxes are similar at 900°C and approximately 2 times higher than those obtained through the dense LSFGa5573 membrane (1 mm thick) without porous layers (Table 3). Jeon et al. [29], Vente et al. [36] and Büchler et al. [37] also reported that oxygen fluxes through asymmetric membranes are only about 2 times higher than for $La_{0.1}Sr_{0.9}Fe_{0.2}Co_{0.8}O_{3-\delta}$, $La_{0.6}Sr_{0.4}Fe_{0.8}Co_{0.2}O_{3-\delta}$ and $La_{0.58}Sr_{0.4}Fe_{0.8}Co_{0.2}O_{3-\delta}$ materials. Moreover, Vente et al. [36] also studied the oxygen semipermeation fluxes of asymmetric $La_{0.6}Sr_{0.4}Fe_{0.8}Co_{0.2}O_{3-\delta}$ membranes with a thin porous layer in contact with oxygen rich or lean side, and they found that fluxes are similar in the two cases, as shown in this work.

The thickness of the dense layer is different between the dense thick membrane and the asymmetric membrane. Some authors [23] [38] [25] studied the influence of the dense layer thickness on oxygen semipermeation fluxes through the membrane. A characteristic thickness L_c, was introduced by Bouwmeester et al. [39], as a criteria to identify the rate-determining step of oxygen transport through the membrane material. If the dense membrane has a low thickness ($10\ L < L_C$), the flux is considered governed only by surface exchanges, whereas if

the dense membrane has a high thickness ($L > 10\ L_C$), the flux is considered governed only by oxygen bulk diffusion.

Nevertheless, the oxygen flux is not inversely proportional to the dense membrane thickness, as expected from the usual Wagner model. The dense layer in the asymmetric membranes (type 1) is five times thinner than the dense membrane without surface modification. Conversely, the oxygen flux through the asymmetric membranes (type 1) is only approximately two times higher than that obtained through the dense LSFGa5573 membrane, suggesting the oxygen flux through asymmetric membranes (type 1) is not only governed by oxygen diffusion, but mainly by surface exchanges. Thus, the thickness of the thick dense membrane is most likely lower than the characteristic thickness L_c defined by Bouwmeester et al. [39].

Jeon et al. [29], Gurauskis et al. [27], Serra et al. [28], Garcia-Torregrosa et al. [40], and Van der Haar [30] reported similar conclusions when the porous support was in contact with the oxygen rich side. Indeed, these authors reported that asymmetric membranes (type 1) show an oxygen flux only 2 to 7 times higher than that obtained for the dense membrane without porous layers (Table 3), while the dense layer in the asymmetric membrane (type 1) is approximately 25 times thinner than the dense membrane without a modification surface.

Moreover, for the asymmetric membranes (type 1), two membranes with a dense layer of 170-230µm and 450-500 µm in thickness, have been characterized with the porous support in contact with air. However, the fluxes through these membranes are similar until 900°C and there is a slight discrepancy between oxygen fluxes above to 900°C (see figure S1). The dense layer thickness of the membrane has then not a significant impact on the oxygen flux through the asymmetric membrane of type 1. This result confirms that the oxygen semipermeation fluxes through dense LSFGa5573 membranes and asymmetric LSFGa5573 membranes of type 1 are mainly governed by oxygen surface exchanges.

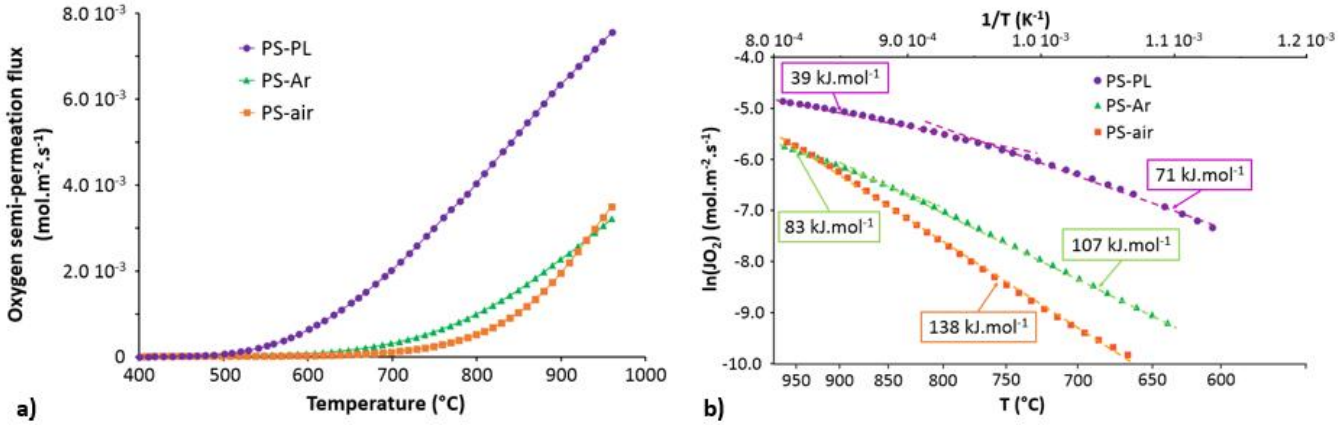

Figure 6: a) Temperature dependence of the oxygen semipermeation fluxes (JO_2) through asymmetric membranes under an air (100 ml.min^{-1})/argon (200 ml.min^{-1}) gradient, b) Arrhenius plots of oxygen fluxes versus *1/T for asymmetric membranes*

Table 3: Activation energies and oxygen semipermeation fluxes through asymmetric membranes of type 1 and dense membranes at 900°C

Dense membrane material/ Thickness	**Support material/Rate of porosity/ Thickness**	**Reference**	**pO_2 in oxygen rich/lean chamber (atm.)**	**Oxygen semi-permeation flux ($mol.m^{-2}.s^{-1}$)**	**Activation energy at high and low temperatures ($kJ.mol^{-1}$)**
PS-air	$La_{0.5}Sr_{0.5}Fe_{0.7}Ga_{0.3}O_{3-\delta}$/ 25-30%/750-800 µm	This work	0.21/3.9 10^{-3}	2.0 10^{-3}	138 (675-960°C)
PS-Ar			0.21/4.6 10^{-3}	2.3 10^{-3}	83 (860-960°C) 107 (675-860°C)
$La_{0.5}Sr_{0.5}Fe_{0.7}Ga_{0.3}O_{3-\delta}$/ 1 mm	-	Guironnet et al. [12] [31]	Air/Argon	8.5-9.5 10^{-4}	120 (820-970°C) 155 (640-820°C)
$La_{0.2}Sr_{0.8}Fe_{0.8}Ta_{0.2}O_{3-\delta}$/ 20 µm	$La_{0.2}Sr_{0.8}Fe_{0.8}Ta_{0.2}O_{3-\delta}$/ 34%/3 mm	Gurauskis et al. [27]	O_2/0.01	2.7 10^{-2}	34 (900-1000°C) 105 (800-900°C)
$La_{0.2}Sr_{0.8}Fe_{0.8}Ta_{0.2}O_{3-\delta}$/ 500 µm	-		O_2/0.01	3.7 10^{-3}	77 (800-1000°C)
$La_{0.1}Sr_{0.9}Fe_{0.2}Co_{0.8}O_{3-\delta}$/ 12 µm	$La_{0.1}Sr_{0.9}Fe_{0.2}Co_{0.8}O_{3-\delta}$/ 28,52%/1 mm	Jeon et al. [29]	0.21/0.01	2.3 10^{-2}	-
$La_{0.1}Sr_{0.9}Fe_{0.2}Co_{0.8}O_{3-\delta}$/ 270 µm	-		0.21/0.01	1.3 10^{-2}	-
$La_{0.6}Sr_{0.4}Fe_{0.8}Co_{0.2}O_{3-\delta}$/ 30 µm	$La_{0.6}Sr_{0.4}Fe_{0.8}Co_{0.2}O_{3-\delta}$/ 39%/630 µm	Serra et al. [28]	Air/Argon	1.8 10^{-2}	72 (850-1000°C) 123 (750-850°C)
$La_{0.6}Sr_{0.4}Fe_{0.8}Co_{0.2}O_{3-\delta}$/ 800 µm	-	Garcia-Torregrosa et al. [40]	Air/Argon	2.6 10^{-3}	89 (850-1000°C) 119 (750-850°C)
$La_{0.5}Sr_{0.5}CoO_{3-\delta}$/ 20 µm	$La_{0.5}Sr_{0.5}CoO_{3-\delta}$/ 30%/500 µm	Van der Haar [30]	Air/He	2.2 10^{-2}	-
$La_{0.5}Sr_{0.5}CoO_{3-\delta}$/ 440 µm	-		Air/He	4.5 10^{-3}	-
$La_{0.6}Sr_{0.4}Fe_{0.8}Co_{0.2}O_{3-\delta}$/ 6 µm	$La_{0.6}Sr_{0.4}Fe_{0.8}Co_{0.2}O_{3-\delta}$/ 12%/200 µm	Vente et al. [36]	Air/He	1.1 10^{-2}	-
$La_{0.6}Sr_{0.4}Fe_{0.8}Co_{0.2}O_{3-\delta}$/ 200 µm	$La_{0.6}Sr_{0.4}Fe_{0.8}Co_{0.2}O_{3-\delta}$/ 35%/10 µm		Air/He	6.1 10^{-3}	-
$La_{0.6}Sr_{0.4}Fe_{0.8}Co_{0.2}O_{3-\delta}$/ 200 µm	-		Air/He	5.8 10^{-3}	-
$La_{0.58}Sr_{0.4}Fe_{0.8}Co_{0.2}O_{3-\delta}$/ 10 µm	$La_{0.58}Sr_{0.4}Fe_{0.8}Co_{0.2}O_{3-\delta}$-$Ce_{0.8}Gd_{0.2}O_{1.9}$/ 36%/ 1.1 mm	Büchler et al. [37]	Air/He	5.5 10^{-4}	133 (750-900°C)
$La_{0.58}Sr_{0.4}Fe_{0.8}Co_{0.2}O_{3-\delta}$/ 1.2 mm	-		Air/He	2.8 10^{-4}	238 (750-900°C)
$La_{0.6}Ca_{0.4}CoO_{3-\delta}$/ 10 µm	$La_{0.6}Ca_{0.4}CoO_{3-\delta}$/-/ 2 mm	Watanabe et al. [41]	Air/He	1.0 10^{-2}	-
$La_{0.6}Ca_{0.4}CoO_{3-\delta}$/ 1.2 mm	-		Air/He	2.9 10^{-3}	-

The activation energies (E_a) of the mechanisms limiting oxygen transport through the membrane architectures at high and low temperatures, determined from Arrhenius plots in Figure 6 b), are reported in Tables 3 and 4. Two ranges of activation energies, one

approximately 40-75 kJ.mol^{-1} and the other approximately 130-180 kJ.mol^{-1}, can be associated with the nature of the rate-determining step (Tables 3 and 4). Indeed, if the oxygen flux is regulated by bulk oxygen diffusion through the membrane, then the activation energy range is between approximately 40 and 75 kJ.mol^{-1}; if the oxygen flux is essentially directed by surface exchanges between the gas and the membrane, then the activation energy is between approximately 130 and 180 kJ.mol^{-1}. Thus, the membrane material's chemical composition does not significantly influence the activation energies of oxygen transport through the membrane, particularly when the oxygen flux is controlled by bulk oxygen diffusion.

In the case of the "PS-air" configuration, only one activation energy was found over this study's full temperature range, suggesting the same rate-determining step in this temperature range. The activation energy is close to that obtained for the dense LSFGa5573 membrane (Table 3) and corresponds to surface exchange mechanisms. Thus, when the porous support is in contact with the oxygen-rich side, the oxygen flux through our asymmetric membranes of type 1 is mainly governed by surface exchanges at the oxygen lean side. Data reported in the literature assume that a decrease in the dense membrane thickness leads to an increase in the oxygen flux and a decrease in the activation energy at high temperature associated with a progressive evolution of the rate-determining step from oxygen surface exchanges to oxygen bulk diffusion (Table 3).

For the "PS-Ar" configuration, two activation energies were observed from the Arrhenius plot, one at high temperature (>860°C) and another at low temperature (<860°C). However, the values of the two activation energies remain close. Thus, there is likely no change in the rate-determining step over the full temperature range in this study. The activation energy at a high temperature of approximately 80 kJ.mol-1 is lower than that obtained for the PS-air architecture and the dense LSFGa5573 membrane. Thus, the porous support allows for a slight increase in the kinetics of exchanges between the gas and the membrane surface, particularly at the oxygen lean side (which is often the limiting step of oxygen transport through the membrane). However, when the porous support is in contact with the oxygen lean side, the gaseous oxygen diffusion through the porous support could also correspond to the rate-determining step mainly for a sizeable porous support thickness. For instance, Guironnet et al. [12] show that a thick porous coating at the surface membrane (up to 100 µm) leads to decreased oxygen semipermeation flux through the membrane. A decrease in the porous layer thickness could then be beneficial to improve oxygen flux and gaseous oxygen diffusion through the porous layer.

In conclusion, when the porous support is in contact with the oxygen-rich side, the oxygen fluxes through the asymmetric membrane of type 1 are likely also governed by surface exchanges at the oxygen lean side (typically with high activation energy: 130-180 kJ.mol^{-1}). However, when the porous support is in contact with the oxygen lean side, the oxygen fluxes through the asymmetric membrane (type 1) are governed by another kind of rate-determining step with lower activation energy, approximately 100 kJ.mol^{-1} (Figure 6 b) and Table 3).

Oxygen semipermeation fluxes through asymmetric membranes of type 1 are mainly governed by oxygen gaseous diffusion through the thick porous support when the support is in contact with the oxygen lean side. Thus, the porous layer thickness in contact with the oxygen lean side has to be decreased to improve the oxygen flux. The second type of asymmetric membrane architecture was then developed from a thick porous support, a thin dense membrane, and a thin porous layer (Figure 1 c). The characteristics of this type 2 asymmetric membrane with a thin porous layer is displayed in Table 2.

Two configurations are possible; either the porous support is in contact with the oxygen rich side and the thin porous layer with the oxygen lean side (configuration A), or the porous support is in contact with the oxygen lean side and the thin porous layer with the oxygen rich side (configuration B). Only the electrochemical performances of the configuration A have been presented in this work. Indeed, the configuration B leads to the rupture of the dense layer during the measurements. This is due to the large chemical expansion of the thin porous layer or the porous support, when it is in contact with the atmosphere with low oxygen partial pressure (or the oxygen lean side). Then, in case of the configuration A, there is not the rupture of thin dense layer solicited in compression. In the case of the configuration B, the thin dense layer is submitted to tensile stresses its fracture.

The oxygen semipermeation flux through the asymmetric membrane of type 2 is shown in Figure 6 a). The flux of 6.3 10^{-3} mol.m^{-2}.s^{-1} reached at 900°C, is approximately three times higher than the one of the asymmetric membrane of type 1 and almost seven times higher than the one obtained from a dense LSFGa5573 membrane without porous layers (Table 4).
However, the data in the literature do not show the same results. Gurauskis et al. [27], Jeon et al. [29] and Watanabe et al. [41] reported that an asymmetric membrane with a thin porous layer (type 2) shows an oxygen flux only slightly higher (approximately 1.2-2 times) than that obtained through the asymmetric membrane of type 1 for LSFTa2882, $CaTi_{0.8}Fe_{0.2}O_{3-\delta}$ and $La_{0.6}Ca_{0.4}CoO_{3-\delta}$ materials (Tables 3 and 4). Figueiredo et al. [42] also observed that the oxygen flux through an asymmetric membrane of type 2 developed from the LSFCo1928 material is only two times higher than that obtained through the dense LSFCo1928 membrane without porous layers, suggesting the materials studied by these authors have high coefficients of surface exchange compared to the LSFGa5573 material.
Furthermore, fluxes reported by Jeon et al. [29] are very high (>1.10^{-2} mol.m^{-2}.s^{-1}), which is surprising for this kind of material.

Table 4: Activation energies and oxygen semipermeation fluxes through asymmetric membranes of type 2 and dense membranes at 900°C

Dense membrane material/ Thickness	**Porous layer material/ Porosity rate/Thickness**	**Reference**	**pO_2 in oxygen rich/lean chamber (atm.)** ***Temperature***	**Oxygen semi-permeation flux (mol.m^{-2}.s^{-1})**	**Activation energy at high and low temperatures (kJ.mol^{-1})**
PS-PL	$La_{0.5}Sr_{0.5}Fe_{0.7}Ga_{0.3}O_{3-\delta}$/ 25-30%/150-	This work	0.21/1.3 10^{-2} *900°C*	6.3 10^{-3}	39 (790-970°C) 71 (600-790°C)

	200 µm				
$La_{0.5}Sr_{0.5}Fe_{0.7}Ga_{0.3}O_{3-\delta}$/ 1 mm	-	Guironnet et al. [12] [31]	Air/Argon *900°C*	8.5-9.5 10^{-4}	120 (820-970°C) 155 (640-820°C)
$CaTi_{0.8}Fe_{0.2}O_{3-\delta}$/ 80 µm	$CaTi_{0.8}Fe_{0.2}O_{3-\delta}$ /20-45%/25-30 µm	Figueiredo et al. [42]	0.21/0.021 *950°C*	7.1 10^{-4}	-
$CaTi_{0.8}Fe_{0.2}O_{3-\delta}$/ 1 mm	-		0.21/0.021 *950°C*	4.2 10^{-4}	-
$La_{0.2}Sr_{0.8}Fe_{0.8}Ta_{0.2}O_{3-\delta}$/ 20 µm	$La_{0.2}Sr_{0.8}Fe_{0.8}Ta_{0.2}O_{3-\delta}$/-/-	Gurauskis et al. [27]	O_2/0.01 *900°C*	3.1 10^{-2}	37 (800-1000°C)
$La_{0.2}Sr_{0.8}Fe_{0.8}Ta_{0.2}O_{3-\delta}$/ 500 µm	-		O_2/0.01 *900°C*	3.7 10^{-3}	77 (800-1000°C)
$La_{0.1}Sr_{0.9}Fe_{0.2}Co_{0.8}O_{3-\delta}$/12 µm	$La_{0.1}Sr_{0.9}Fe_{0.2}Co_{0.8}O_{3-\delta}$/20.45%/20 µm	Jeon et al. [29]	0.21/0.01 *900°C*	2.7 10^{-2}	-
$La_{0.1}Sr_{0.9}Fe_{0.2}Co_{0.8}O_{3-\delta}$/270 µm	-		0.21/0.01 *900°C*	1.3 10^{-2}	-
$La_{0.6}Ca_{0.4}CoO_{3-\delta}$/ 10 µm	$La_{0.6}Ca_{0.4}CoO_{3-\delta}$/-/ 10 µm	Watanabe et al. [41]	Air/He	2.3 10^{-2}	-
$La_{0.6}Ca_{0.4}CoO_{3-\delta}$/ 1.2 mm	-		Air/He	2.9 10^{-3}	-

Figure 6 b) shows the Arrhenius plot of oxygen semipermeation flux versus 1/T (T: absolute temperature in K) for asymmetric membranes with thin porous layers (type 2). Two activation energies of mechanisms limiting oxygen transport can be determined from the Arrhenius plot, one at high temperature (>790°C) corresponding to mechanisms of oxygen bulk diffusion and another at low temperature (<790°C) likely cor

responding to a mixed regimen (Table 4). There is a change of limiting step, approximately 790°C. At high temperatures, the activation energy of the PS-PL architecture of 39 $kJ.mol^{-1}$ is much lower than that of the dense LSFGa5573 membrane without porous layers and similar to the activation energy reported by Gurauskis et al. [27] for a similar membrane architecture developed from the LSFTa2882 material.

Thus, a decrease in the porous layer's thickness in contact with the oxygen lean side allows a significant increase in oxygen gaseous diffusion through the porous layer.

3.3 Rate-determining step of oxygen transport through symmetric and asymmetric membranes

The first architecture of the membrane (symmetric membrane), composed of a dense LSFGa5573 membrane (1 mm) and thin BSF55 coatings on both sides, shows high oxygen semipermeation fluxes compared to the dense LSFGa5573 membrane without surface modification. Oxygen fluxes through the symmetric membrane are governed by oxygen bulk diffusion at high temperature (>860°C).

The second architecture (asymmetric membrane of type 1) is composed of a thin dense LSFGa5573 layer (150-200 µm) supported by thick porous support developed from wood flour. This work shows that the decrease in the dense layer thickness does not significantly

improve oxygen fluxes through the membrane if the membrane material has high oxygen bulk diffusion coefficients, such as the LSFGa5573 material. This trend also suggests that, in the case of an asymmetric membrane of type 1, gaseous oxygen diffusion through thick porous support in contact with the oxygen lean side can also be the rate-determining step of oxygen transport.
The last membrane architecture (asymmetric membrane of type 2) comprises thick porous support developed from wood flour in contact with the oxygen-rich side, a thin dense layer, and a thin porous layer produced from wood flour in contact with the oxygen lean side. This asymmetric membrane with a thin porous layer shows very high oxygen semipermeation fluxes compared to the dense LSFGa5573 membrane without surface modification. Oxygen fluxes through this asymmetric membrane are then governed by oxygen bulk diffusion at high temperature (>790°C).
Thus, a thin porous layer in contact with the oxygen lean side allows significant enhancement of oxygen gaseous diffusion through the porous layer and kinetics of exchanges between the gas and the membrane surface if the membrane material shows low coefficients of surface exchanges, such as the LSFGa5573 material. Table 5 summarizes the main results of this work.

Figure 7 shows oxygen semipermeation fluxes through these different membrane architectures, which are compared with fluxes obtained through 1 mm-thick dense LSFGa5573 [12] [31] and $Ba_{0.5}Sr_{0.5}Fe_{0.2}Co_{0.8}O_{3-\delta}$ (BSFCo5528) membranes [34]. The oxygen flux obtained for the asymmetric membrane of type 2 (with a thin porous layer) is close to that obtained for the dense BSFCo5528 membrane [34] under the same working conditions and slightly lower than the oxygen flux through the 1 mm-thick dense BSFCo5528 membrane obtained in the literature at 900°C with a grain size of approximately 10-15 µm [8].

Table 5: Characteristics of membrane architectures studied in this work and by Guironnet et al. *[12] [31]*

Membrane architecture	**Oxygen semi-permeation flux ($mol.m^{-2}.s^{-1}$)**	**Activation energy at high and low temperatures ($kJ.mol^{-1}$)**	**Rate-determining step**
Dense LSFGa5573 membrane	$8.5\text{-}9.5\ 10^{-4}$	120 (820-970°C) 155 (640-820°C)	Oxygen surface exchanges
Symmetric LSFGa5573/BSF55 membrane	$3.4\ 10^{-3}$	57 (760-960°C) 75 (600-760°C)	Oxygen bulk diffusion
Asymmetric membrane of type 1 (without thin porous layer)	$2.3\ 10^{-3}$	83 (860-960°C) 107 (675-860°C)	Oxygen gaseous diffusion
Asymmetric membrane of type 2 (with thin porous layer)	$6.3\ 10^{-3}$	39 (790-970°C) 71 (600-790°C)	Oxygen bulk diffusion

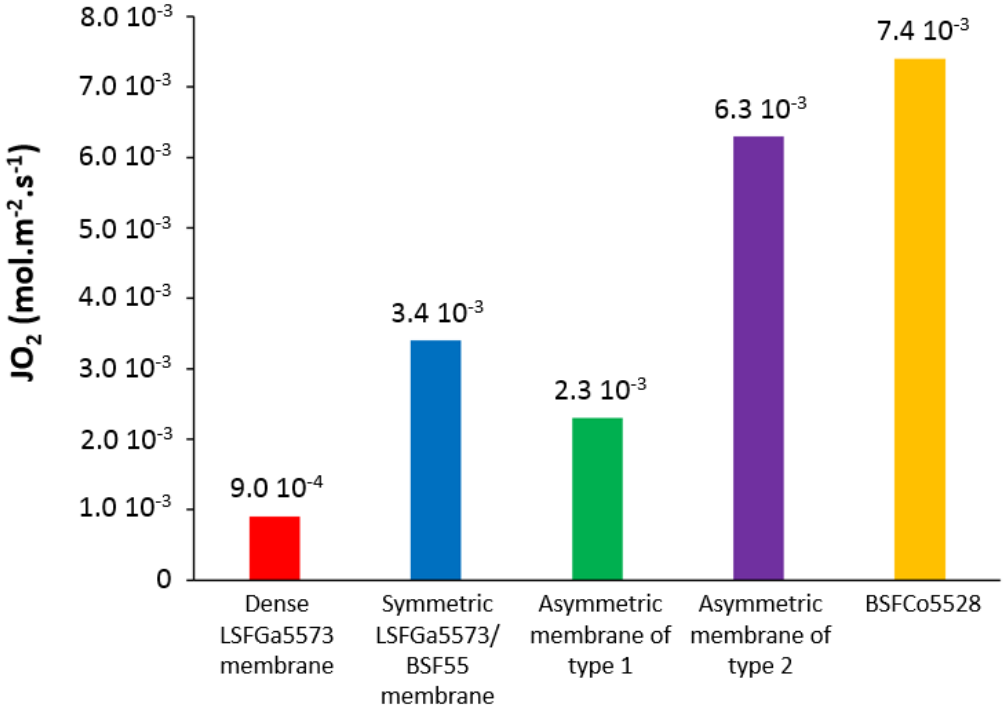

Figure 7: Oxygen semipermeation fluxes (JO_2) through membrane architectures studied in this work and through the 1 mm-thick dense LSFGa5573 [12] [31] and BSFCo5528 membranes [34] at 900°C under an air (100 ml.min^{-1})/argon (200 ml.min^{-1}) gradient

4 Conclusion

Three membrane architectures were developed from LSFGa5573 and BSF55 materials and characterized by a semipermeation method.

LSFGa5573 material was used for the dense layer concerning symmetric membranes because this material has high oxygen bulk diffusion coefficients and high mechanical properties. The BSF55 material was used for coatings because it shows high oxygen surface exchange coefficients but low mechanical properties.

Concerning asymmetric membranes, the thin dense LSFGa5573 layer was supported by a thick porous layer of the same material. The other surface of the thin dense LSFGa5573 layer was coated or not by a thin porous LSFGa5573 layer.

The rate-determining step of oxygen transport depends strongly on the membrane architecture and membrane materials, and the dense layer's thickness.

In addition, in the case of asymmetric membranes of type 1 (without a thin porous layer), gaseous oxygen diffusion through the thick porous support corresponds to the potential rate-determining step of oxygen transport, which is not clearly identified in the literature.

The asymmetric membrane of type 2 (with a thin porous layer) is the optimal architecture corresponding to the best compromise between high mechanical properties and high oxygen semipermeation performance. This architecture shows an oxygen flux of 6.3 10^{-3} mol.m^{-2}.s^{-1} at 900°C, almost 7 times higher than that obtained from a dense LSFGa5573 membrane without porous layers.

5 References

[1] P.-M. Geffroy, E. Blond, N. Richet, T. Chartier, Understanding and identifying the oxygen transport mechanisms through a mixed-conductor membrane, Chemical Engineering Science. 162 (2017) 245–261. https://doi.org/10.1016/j.ces.2017.01.006.

[2] M. Lipińska-Chwałek, F. Schulze-Küppers, J. Malzbender, Strength and elastic modulus of lanthanum strontium cobalt ferrite membrane materials, Ceramics International. 41 (2015) 1355–1360. https://doi.org/10.1016/j.ceramint.2014.09.068.

[3] P.M. Geffroy, M. Reichmann, L. Kilmann, J. Jouin, N. Richet, T. Chartier, Identification of the rate-determining step in oxygen transport through La(1−x)SrxFe(1−y)GayO3−δ perovskite membranes, Journal of Membrane Science. 476 (2015) 340–347. https://doi.org/10.1016/j.memsci.2014.11.048.

[4] J.H. Park, K.Y. Kim, S.D. Park, Oxygen permeation and stability of La0.6Sr0.4TixFe1−xO3−δ (x = 0.2 and 0.3) membrane, Desalination. 245 (2009) 559–569. https://doi.org/10.1016/j.desal.2009.02.021.

[5] M. Brisotto, F. Cernuschi, F. Drago, C. Lenardi, P. Rosa, C. Meneghini, M. Merlini, C. Rinaldi, High temperature stability of Ba0.5Sr0.5Co0.8Fe0.2O3−δ and La0.6Sr0.4Co1−yFeyO3−δ oxygen separation perovskite membranes, Journal of the European Ceramic Society. 36 (2016) 1679–1690. https://doi.org/10.1016/j.jeurceramsoc.2016.01.029.

[6] E. Deronzier, T. Chartier, P.-M. Geffroy, Oxygen semi-permeation properties of La1−xSrxFeO3−δ perovskite membranes under high oxygen gradient, Journal of Materials Research. 35 (2020) 2506–2515. https://doi.org/10.1557/jmr.2020.230.

[7] A. Chanda, B.X. Huang, J. Malzbender, R.W. Steinbrech, Micro- and macro-indentation behaviour of Ba0.5Sr0.5Co0.8Fe0.2O3−d perovskite, Journal of the European Ceramic Society. 31 (2011) 401–408. https://doi.org/10.1016/j.jeurceramsoc.2010.10.022.

[8] T. Klande, O. Ravkina, A. Feldhoff, Effect of microstructure on oxygen permeation of Ba0.5Sr0.5Co0.8Fe0.2O3−δ and SrCo0.8Fe0.2O3−δ membranes, Journal of the European Ceramic Society. 33 (2013) 1129–1136. https://doi.org/10.1016/j.jeurceramsoc.2012.11.023.

[9] H. Wang, C. Tablet, A. Feldhoff, J. Caro, Investigation of phase structure, sintering, and permeability of perovskite-type Ba0.5Sr0.5Co0.8Fe0.2O3−δ membranes, Journal of Membrane Science. 262 (2005) 20–26. https://doi.org/10.1016/j.memsci.2005.03.046.

[10] W.K. Hong, G.M. Choi, Oxygen permeation of BSCF membrane with varying thickness and surface coating, Journal of Membrane Science. 346 (2010) 353–360. https://doi.org/10.1016/j.memsci.2009.09.056.

[11] H. Wang, Y. Cong, W. Yang, Oxygen permeation study in a tubular Ba0.5Sr0.5Co0.8Fe0.2O3-δ oxygen permeable membrane, Journal of Membrane Science. 210 (2002) 259–271. https://doi.org/10.1016/S0376-7388(02)00361-7.

[12] L. Guironnet, P.-M. Geffroy, F. Jouay, C. Pagnoux, N. Richet, T. Chartier, La0.6Sr0.4Fe0.8Co0.2O3-δ electrophoretic coating for oxygen transport membranes,

Chemical Engineering Science: X. 1 (2019) 100008. https://doi.org/10.1016/j.cesx.2019.100008.

[13] K.S. Lee, S. Lee, J.W. Kim, S.K. Woo, Enhancement of oxygen permeation by La0.6Sr0.4CoO3−δ coating in La0.7Sr0.3Ga0.6Fe0.4O3−δ membrane, Desalination. 147 (2002) 439–444. https://doi.org/10.1016/S0011-9164(02)00640-9.

[14] P.L. Rachadel, J. Motuzas, R.A.F. Machado, D. Hotza, J.C. Diniz da Costa, Influence of porous structures on O2 flux of BSCF asymmetric membranes, Separation and Purification Technology. 175 (2017) 164–169. https://doi.org/10.1016/j.seppur.2016.10.053.

[15] P. Niehoff, S. Baumann, F. Schulze-Küppers, R. Bradley, I. Shapiro, W.A. Meulenberg, P. Withers, R. Vaßen, Oxygen transport through supported Ba0.5Sr0.5Co0.8Fe0.2O3−δ membranes, Separation and Purification Technology. 121 (2014) 60–67. https://doi.org/10.1016/j.seppur.2013.07.002.

[16] X. Li, T. Kerstiens, T. Markus, Oxygen permeability and phase stability of Ba0.5Sr0.5Co0.8Fe0.2O3−δ perovskite at intermediate temperatures, Journal of Membrane Science. 438 (2013) 83–89. https://doi.org/10.1016/j.memsci.2013.03.017.

[17] W. Jin, S. Li, P. Huang, N. Xu, J. Shi, Preparation of an asymmetric perovskite-type membrane and its oxygen permeability, Journal of Membrane Science. 185 (2001) 237–243. https://doi.org/10.1016/S0376-7388(00)00650-5.

[18] M. Betz, F. Schulze-Küppers, S. Baumann, W.A. Meulenberg, D. Stöver, Supported Oxygen Transport Membranes for Oxyfuel Power Plants, Advances in Science and Technology. 72 (2010) 93–98. https://doi.org/10.4028/www.scientific.net/AST.72.93.

[19] Z. Cao, X. Zhu, W. Li, B. Xu, L. Yang, W. Yang, Asymmetric dual-phase membranes prepared via tape-casting and co-lamination for oxygen permeation, Materials Letters. 147 (2015) 88–91. https://doi.org/10.1016/j.matlet.2015.02.033.

[20] S. Guo, Z. Liu, J. Zhu, X. Jiang, Z. Song, W. Jin, Highly oxygen-permeable and CO2-stable Ce0.8Sm0.2O2−δ-SrCo0.9Nb0.1O3−δ dual-phase membrane for oxygen separation, Fuel Processing Technology. 154 (2016) 19–26. https://doi.org/10.1016/j.fuproc.2016.07.009.

[21] K. Partovi, C.H. Rüscher, F. Steinbach, J. Caro, Enhanced oxygen permeability of novel Cu-containing CO2-tolerant dual-phase membranes, Journal of Membrane Science. 503 (2016) 158–165. https://doi.org/10.1016/j.memsci.2016.01.019.

[22] X. Bi, X. Meng, P. Liu, N. Yang, Z. Zhu, R. Ran, S. Liu, A novel CO2-resistant ceramic dual-phase hollow fiber membrane for oxygen separation, Journal of Membrane Science. 522 (2017) 91–99. https://doi.org/10.1016/j.memsci.2016.09.008.

[23] C. Li, W. Li, J.J. Chew, S. Liu, X. Zhu, J. Sunarso, Rate determining step in SDC-SSAF dual-phase oxygen permeation membrane, Journal of Membrane Science. 573 (2019) 628–638. https://doi.org/10.1016/j.memsci.2018.12.044.

[24] W. He, J. Liu, C. Chen, M. Ni, Oxygen permeation modeling for Zr0.84Y0.16O1.92–La0.8Sr0.2Cr0.5Fe0.5O3−δ asymmetric membrane made by phase-inversion, Journal of Membrane Science. C (2015) 90–98. https://doi.org/10.1016/j.memsci.2015.05.026.

[25] Y. Zhang, R. Yuan, J. Gao, C. Chen, Oxygen permeation properties of supported planar Zr0.84Y0.16O1.92-La0.8Sr0.2Cr0.5Fe0.5O3−δ composite membranes, Separation and Purification Technology. 166 (2016) 142–147. https://doi.org/10.1016/j.seppur.2016.04.029.

[26] C. Li, X. Ban, C. Chen, Z. Zhan, Sandwich-like symmetric dual-phase composite membrane with an ultra-thin oxygen separation layer and excellent durability, Solid State Ionics. 345 (2020) 115176. https://doi.org/10.1016/j.ssi.2019.115176.

[27] J. Gurauskis, Ø.F. Lohne, D.S. Lagergren, E.T. Wefring, K. Wiik, Oxygen permeation in symmetric and asymmetric La0.2Sr0.8Fe0.8Ta0.2O3−δ membranes, Journal of the European Ceramic Society. 36 (2016) 1427–1434. https://doi.org/10.1016/j.jeurceramsoc.2016.01.004.

[28] J.M. Serra, J. Garcia-Fayos, S. Baumann, F. Schulze-Küppers, W.A. Meulenberg, Oxygen permeation through tape-cast asymmetric all-La0.6Sr0.4Co0.2Fe0.8O3−δ membranes, Journal of Membrane Science. 447 (2013) 297–305. https://doi.org/10.1016/j.memsci.2013.07.030.

[29] S.-Y. Jeon, H.-N. Im, B. Singh, M. Choi, Y.-S. Yoo, J.-H. Hwang, S.-J. Song, Oxygen permeation through dense La0.1Sr0.9Co0.8Fe0.2O3−δ perovskite membranes: Catalytic effect of porous La0.1Sr0.9Co0.8Fe0.2O3−δ layers, Ceramics International. 41 (2015) 7446–7452. https://doi.org/10.1016/j.ceramint.2015.02.064.

[30] Marco van der Haar, Mixed-conducting perovskite membranes for oxygen separation, thesis, Universiteit Twente. (n.d.), 2001. https://www.utwente.nl/en/tnw/ims/publications/former-phd/files/mha/ (accessed May 3, 2021).

[31] L. Guironnet, P.-M. Geffroy, N. Tessier-Doyen, A. Boulle, N. Richet, T. Chartier, The surface roughness effect on electrochemical properties of La0.5Sr0.5Fe0.7Ga0.3O3-δ perovskite for oxygen transport membranes, Journal of Membrane Science. 588 (2019) 117199. https://doi.org/10.1016/j.memsci.2019.117199.

[32] A. Vivet, P.M. Geffroy, T. Chartier, P. Del Gallo, N. Richet, La(1−x)SrxFe(1−y)GayO3−δ perovskite membrane: Oxygen semi-permeation, thermal expansion coefficient and chemical stability under reducing conditions, Journal of Membrane Science. 372 (2011) 373–379. https://doi.org/10.1016/j.memsci.2011.02.021.

[33] A. Julian, E. Juste, P.M. Geffroy, V. Coudert, S. Degot, P. Del Gallo, N. Richet, T. Chartier, Elaboration of La0.8Sr0.2Fe0.7Ga0.3O3−δ/La0.8M0.2FeO3−δ (M=Ca, Sr and Ba) asymmetric membranes by tape-casting and co-firing, Journal of Membrane Science. 333 (2009) 132–140. https://doi.org/10.1016/j.memsci.2009.02.002.

[34] M. Reichmann, P.-M. Geffroy, N. Richet, T. Chartier, Impact of microstructure on oxygen semi-permeation performance of perovskite membranes: Understanding of oxygen transport mechanisms, Journal of Power Sources. 324 (2016) 774–779. https://doi.org/10.1016/j.jpowsour.2016.06.009.

[35] H. Pan, L. Li, X. Deng, B. Meng, X. Tan, K. Li, Improvement of oxygen permeation in perovskite hollow fibre membranes by the enhanced surface exchange kinetics, Journal of Membrane Science. 428 (2013) 198–204. https://doi.org/10.1016/j.memsci.2012.10.020.

[36] J.F. Vente, W.G. Haije, Z.S. Rak, Performance of functional perovskite membranes for oxygen production, Journal of Membrane Science. 276 (2006) 178–184. https://doi.org/10.1016/j.memsci.2005.09.046.

[37] O. Büchler, J.M. Serra, W.A. Meulenberg, D. Sebold, H.P. Buchkremer, Preparation and properties of thin La1−xSrxCo1−yFeyO3−δ perovskitic membranes supported on tailored ceramic substrates, Solid State Ionics. 178 (2007) 91–99. https://doi.org/10.1016/j.ssi.2006.11.015.

[38] C. Li, W. Li, J.J. Chew, S. Liu, X. Zhu, J. Sunarso, Oxygen permeation through single-phase perovskite membrane: Modeling study and comparison with the dual-phase membrane, Separation and Purification Technology. 235 (2020) 116224. https://doi.org/10.1016/j.seppur.2019.116224.

[39] H.J.M. Bouwmeester, Dense ceramic membranes for methane conversion, Catalysis Today. 82 (2003) 141–150. https://doi.org/10.1016/S0920-5861(03)00222-0.

[40] I. García- Torregrosa, M.P. Lobera, C. Solís, P. Atienzar, J.M. Serra, Development of CO2 Protective Layers by Spray Pyrolysis for Ceramic Oxygen Transport Membranes, Advanced Energy Materials. 1 (2011) 618–625. https://doi.org/10.1002/aenm.201100169.

[41] K. Watanabe, M. Yuasa, T. Kida, K. Shimanoe, Y. Teraoka, N. Yamazoe, Preparation of oxygen evolution layer/La0.6Ca0.4CoO3 dense membrane/porous support asymmetric structure for high-performance oxygen permeation, Solid State Ionics. 179 (2008) 1377–1381. https://doi.org/10.1016/j.ssi.2007.12.092.

[42] F.M. Figueiredo, V.V. Kharton, A.P. Viskup, J.R. Frade, Surface enhanced oxygen permeation in CaTi1−xFexO3−δ ceramic membranes, Journal of Membrane Science. 236 (2004) 73–80. https://doi.org/10.1016/j.memsci.2004.02.008.

Figure captions

Table captions